

High-Yield Preparation of Exfoliated 1T-MoS₂ with SERS Activity

Engin Er,^{†,‡} Hui-Lei Hou,[†] Alejandro Criado,^{*,†} Judith Langer,[†] Marco Möller,[†] Nevin Erk,[‡] Luis M. Liz-Marzán,^{†,§} and Maurizio Prato^{*,†,§,||}

[†]CIC biomaGUNE, Paseo de Miramón, 182, Donostia-San Sebastián 20014, Spain

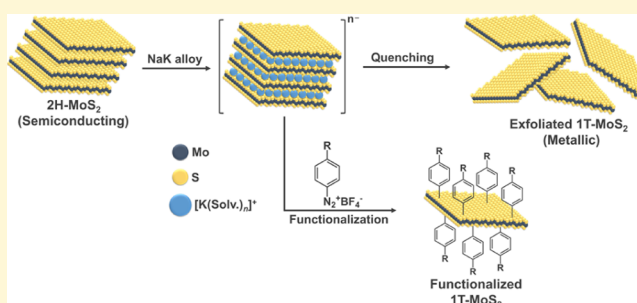
[‡]Department of Analytical Chemistry, Faculty of Pharmacy, Ankara University, Ankara 06560, Turkey

[§]Ikerbasque, Basque Foundation for Science, Bilbao 48013, Spain

^{||}Department of Chemical and Pharmaceutical Sciences, Università degli Studi di Trieste, Via Licio Giorgieri 1, Trieste 34127, Italy

S Supporting Information

ABSTRACT: Molybdenum disulfide (MoS₂), a promising two-dimensional transition-metal dichalcogenide, presents a challenge in the tuning of its optoelectronic and chemical properties. Herein, we demonstrate an efficient route to alter the crystalline structure of MoS₂ by chemical exfoliation. Using NaK metal alloys, exfoliated and covalently functionalized MoS₂ derivatives were obtained with a high metallic (1T) phase ratio, up to 94.5%. Consequently, exfoliated MoS₂ showed a significant surface-enhanced Raman scattering activity toward rhodamine 6G (R6G) and crystal violet, with low detection limits. The versatility of this approach allows the covalent functionalization of MoS₂ without relying on edge or basal-plane defects of the structure and preserving the high-ratio 1T phase.



INTRODUCTION

Since the discovery of graphene, two-dimensional (2D) layered transition-metal dichalcogenides (TMDs) have attracted great attention because of their interesting properties in various application fields, such as electronic and sensor devices, energy-storage, catalysis, and composite materials.^{1–5} Molybdenum disulfide (MoS₂), one of the most interesting 2D materials, features properties such as a direct band gap (1.9 eV) and high carrier mobility (200–500 cm² V⁻¹ s⁻¹), as well as interesting optical properties, such as surface-enhanced Raman scattering (SERS) and high thermal stability.^{6,7}

MoS₂ is commonly found as a polytype involving the 2H phase (2H-MoS₂) with semiconducting properties and the 1T phase (1T-MoS₂) with metallic properties.⁸ 1T-MoS₂ features conductivity up to 10⁷ times higher than 2H-MoS₂, as well as superior charge transfer (CT) ability. Therefore, the metallic phase of MoS₂ may find applications including supercapacitors, hydrogen evolution reaction, and SERS.^{9–12}

SERS is one of the most selective and ultrasensitive analytical techniques in bioimaging and biosensing¹³ because of the unique vibrational fingerprints of the target molecules and low detection limits. The common SERS phenomenon mainly relies on the so-called electromagnetic (EM) enhancement via localized surface plasmon resonances induced at the surface of metal nanostructures to improve the sensitivity. On the other hand, chemical enhancement (CE) in SERS, which is based on interface dipole–dipole interactions at the substrate as well as CT resonances between the substrate and analyte, is considered as the dominant enhancement mechanism in 2D

materials such as graphene and TMDs.^{14,15} In this context, MoS₂ has been shown to display unusually efficient SERS-enhancing properties,¹⁶ with the dominant contribution being supported by CT resonances. The CT mechanism for different dye molecules (copper phthalocyanine, CuPc, rhodamine 6G, R6G, and crystal violet, CV) has been described as a two-step process, where (I) electrons are excited from the highest occupied molecular orbital (HOMO) into the lowest unoccupied molecular orbital of the dye, leaving holes in the HOMO level, and subsequently, (II) electrons migrate from the valence band edge of the MoS₂ material into the HOMO, thus recombining with holes.¹⁷ Thereby, the SERS response significantly depends on the phase state in which the material is presented. Although step (II) in the semiconductor phase requires an extra energy to transfer electrons from the low-lying valence band edge, in the metallic 1T phase, the higher-lying Fermi electrons could migrate without extra energy into the HOMO. The resulting higher electron transition probability leads to a higher SERS enhancement.^{10,17}

The preparation of the MoS₂ 1T phase with high purity is thus crucial toward improving applications that require high conductivity and effective CT. However, current methods do not allow the production of a pure 1T phase MoS₂ material by any simple approach, because of stability issues and moderately effective processes.^{8,18,19} Ding et al. produced a pure MoS₂ 1T

Received: April 30, 2019

Revised: July 17, 2019

Published: July 17, 2019

phase by a hydrothermal process in the presence of a magnetic field, using harsh conditions.²⁰ In this approach, the considerably high magnetic field (up to 10 T) and temperature used in the synthesis of 1T-MoS₂ hinder the applicability of this method and the large-scale production of 1T-MoS₂. On the other hand, the 1T phase (octahedral), which is metastable, readily converts into the stable 2H phase (trigonal prismatic). This limitation has hindered progress regarding the preparation of 1T-MoS₂. Existing approaches include chemical exfoliation, electron-beam irradiation, electron transfer of plasma hot electrons, mechanical strain, colloidal synthesis, and hydrothermal reaction.^{8,18} Nevertheless, most of the reported methods were shown to produce only mixtures of 1T and 2H phase MoS₂ nanomaterials.

In general, the most useful and effective methodology to prepare 1T-MoS₂ on a large scale is chemical exfoliation.^{19,21,22} In this approach, metal ions (M: Na, K, or Li) are intercalated between MoS₂ layers and then isolated by ultrasound-assisted hydration to achieve the 1T phase in high yield. The intercalating agents lead to partial conversion of the crystal structure from the 2H to the 1T phase, due to electron transfer from the metal ions.²³ The highest reported 1T phase ratio of MoS₂ exfoliated by *n*-butyllithium (*n*-BuLi), the most common intercalating agent for TMD exfoliation, has been ~60–65%.^{24,25} Recently, the electrochemical exfoliation of MoS₂ has also been performed by lithium-ion intercalation under ambient conditions, and the corresponding 1T phase ratio was only 40%.²⁶ Interestingly, even though metal alloys comprising Na and K are rich electron sources, they remain unexplored in terms of phase engineering for TMDs.²⁷

We report herein a highly efficient and simple route to obtain 1T-MoS₂ by metal intercalation with NaK alloys, followed by surface functionalization without using structural defects. This reducing agent, which has excessive negative charges, facilitates MoS₂ exfoliation, with a significantly higher ratio of 1T phase compared to previous reports.^{19,24,25} Consequently, the exfoliated 1T-MoS₂ material was used as a SERS platform for the detection of various probe molecules. Our SERS results demonstrate that 1T-MoS₂ significantly increases the Raman signal of probe molecules through efficient CT.¹⁰ Furthermore, the obtained negatively charged 1T-MoS₂ layers feature the versatility to chemically modify the MoS₂ structures for potential sensing applications.

EXPERIMENTAL SECTION

General. MoS₂ (~6 μm) powder, iodine (I₂; 99.8%), *n*-butyllithium (2.5 M in hexane), 4-fluoroaniline (99%), 4-chloroaniline (98%), 4-bromobenzenediazonium tetrafluoroborate (96%), and 4-nitrobenzenediazonium tetrafluoroborate (97%) were purchased from Sigma-Aldrich. All chemicals including organic solvents used in the reaction and purification were purchased from either Sigma-Aldrich or Alfa-Aesar and used as received. Bulk-MoS₂ was prepared from a suspension of MoS₂ powder (5 mg) in Milli-Q water (5 mL). The resulting suspension was then sonicated (Ultrasons-H Selecta) for 1 h. Centrifugation was carried out (Heraeus Megafuge 16R) at 500 rpm to precipitate the larger flakes. After centrifugation, the top two-thirds of the dispersion were extracted by a pipet. The obtained suspension was filtered (PTFE Millipore filter, 0.45 μm pore size) and dried under vacuum to obtain bulk-MoS₂ (1 mg).

Chemical Exfoliation. MoS₂ powder was dried at 150 °C under vacuum overnight prior to use. Our chemical exfoliating 1T-MoS₂ preparation was a modification of the method reported by Feng et al.²⁷ Briefly, Na (35 mg, 1.5 mmol) and K (59 mg, 1.5 mmol) metals were mixed with 1,2-dimethoxyethane (DME) solution (20 mL) and vigorously stirred for 2 h at room temperature to obtain a liquid NaK

alloy dispersion with a blue color. Then, MoS₂ powder (160 mg, 1 mmol) is added to this solution, and the mixture is allowed to stir for 24 h. The reaction is then quenched by the addition of I₂ (761 mg; 3 mmol) to the stirring solution. The mixture is washed three times with cyclohexane/water (1:1, v/v) solution and then filtered thoroughly using polytetrafluoroethylene (PTFE; 0.45 μm) membrane filters with dimethylformamide (DMF; 4 × 30 mL), ethanol (2 × 20 mL), acetone (2 × 20 mL) and water (2 × 20 mL).

For comparison, the chemical exfoliation of MoS₂ was also performed by *n*-BuLi, in a similar method as reported by Knirsch et al.²⁴ *n*-BuLi solution (3 mL, 2.5 M in hexane) is added to the 200 mg MoS₂ suspension in dry hexane (10 mL) and allowed to stir under an inert atmosphere for 24 h. The black precipitate was filtered thoroughly with dry hexane to remove the unreacted *n*-BuLi and organic impurities and followed by quenching of the reaction with 100 mL of Milli-Q water. The resulting MoS₂ suspension was centrifuged at 750 rpm for 1.5 h to remove the nonexfoliated material and then filtered thoroughly using PTFE (0.45 μm) membrane filters with Milli-Q water.

Diazonium Salt Synthesis. 4-Fluorobenzenediazonium tetrafluoroborate and 4-chlorobenzenediazonium tetrafluoroborate were synthesized from precursors such as 4-fluoroaniline and 4-chloroaniline following the published diazotization procedure (Scheme S1).²⁸ First, 4-fluoroaniline (1 mmol) was added to into HBF₄ aqueous solution (0.4 mL). Then, 40 mL of acetic acid was added and isoamylnitrite (0.4 mL; 3 mmol) solution dissolved in 20 mL acetic acid was slowly added dropwise to the mixture. The reaction was stirred for 15 min at room temperature. The mixture was then quenched by adding of 40 mL of diethyl ether solution and stored at -22 °C overnight. The resultant product was filtered via PTFE filter (0.45 μm) and then washed several times with diethyl ether. The obtained 4-fluorobenzenediazonium tetrafluoroborate was dried under vacuum at room temperature. The 4-chlorobenzenediazonium tetrafluoroborate was prepared by same diazotization procedure as presented above. The Fourier-transform infrared spectroscopy (FTIR) spectra of 4-fluorobenzenediazonium tetrafluoroborate and 4-chlorobenzenediazonium tetrafluoroborate show the characteristic bands of diazonium salt at around 2270 cm⁻¹ as presented in Figure S1.

Covalent Functionalization. For covalent functionalization of MoS₂, MoS₂ intercalated with the NaK alloy as described in the chemical exfoliation paragraph was reacted with 4-fluorobenzenediazonium tetrafluoroborate (630 mg; 3 mmol), 4-chlorobenzenediazonium tetrafluoroborate (680 mg; 3 mmol), 4-bromobenzenediazonium tetrafluoroborate (812 mg; 3 mmol), and 4-nitrobenzenediazonium tetrafluoroborate (711 mg; 3 mmol). After the reaction, each of the resulting precipitates were filtered thoroughly using the PTFE (0.45 μm) membrane filters with DMF (4 × 30 mL), ethanol (2 × 20 mL), acetone (2 × 20 mL), and water (2 × 20 mL). The exfoliated and functionalized MoS₂ materials were then dried under vacuum for the structural and morphological characterizations.

Characterization of Exfoliated Materials. To evaluate the exfoliation of the bulk crystal of the layered MoS₂ precursor (bulk-MoS₂), the exfoliated materials were measured by X-ray diffraction (XRD) and transmission electron microscopy (TEM). XRD analyses were carried out in a Bruker D8 Advance diffractometer with an X-ray source of Cu Kα (1600 W). The diffractometer presents Bragg–Brentano θ–θ configuration for powder samples. TEM images were obtained using a JEOL JEM-1400PLUS electron microscope at 120 kV equipped with a GATAN US1000 CCD camera. High-resolution TEM (HRTEM) images and selected area electron diffraction (SAED) patterns were acquired with a JEOL JEM-2100F UHR electron microscope at 200 kV equipped with a TVIPS F-216 CMOS camera. The TEM samples were prepared by drop-casting sample solutions on the ultrathin carbon film-coated Cu-grids (Ted Pella Inc., USA) and desiccated under ambient conditions.

The change of crystallinity was detected by Raman spectroscopy, X-ray photoelectron spectroscopy (XPS) and UV–vis spectroscopy (UV). Raman spectra were recorded with a Renishaw inVia Raman microscope equipped with laser wavelengths λ = 532, 633, and 785

nm, a lens-based spectrometer with two gratings (1800 gr/mm for vis and 1200 gr/mm for near infrared), and a Peltier-cooled front-illuminated CCD (1024 px × 532 px). XPS measurements were performed in a SPECS Sage HR 100 spectrometer with a nonmonochromatic X-ray source of aluminium with a $K\alpha$ line of 1486.6 eV energy and 300 W. XPS measurements were performed in a SPECS Sage HR 100 spectrometer with a nonmonochromatic X-ray source of aluminium with a $K\alpha$ line of 1486.6 eV energy and 300 W. The fitting of the XPS data was applied using CasaXPS software. The quantification of the 1T phase was calculated by the deconvolution of Mo 3s core levels. UV–visible spectra were studied in a Jasco V-630 BIO or Varian Cary 5000 spectrophotometer.

The chemical modification of MoS₂ was characterized by Raman spectroscopy, XPS, thermogravimetric analysis (TGA), and FTIR. TGA measurements were performed on a TA Instruments Discovery system under air starting from 100 °C with ramp of 10 °C/min up to 800 °C after an isotherm at 100 °C for 20 min. The functionalization degree (FD) for all functionalized samples was calculated by considering the decomposition of MoS₂ at 650 °C in the corresponding TGA profiles (eq 1). FD is expressed in terms of number of MoS₂ molecules per introduced functional group. R and L are corresponded to the weight loss (%) and residue (%) observed at 650 °C, after having subtracted the analogous loss from the pristine MoS₂. The expected moiety on the MoS₂ surface is expressed as (M_w), and the molecular weight of MoS₂ determined to be 160.07 g/mol.

$$FD = \frac{R(\%) \cdot M_w(\text{g/mol})}{L(\%) \cdot 160.07(\text{g/mol})} \quad (1)$$

The FTIR characterization was carried out in transmission mode by means of a Nicolet 6700 spectrometer. For this purpose, solid MoS₂ powders (2 mg) were mixed with a 200 mg KBr matrix, stored in the oven at 80 °C, pestle, and pressed to discs (diameter 13 mm) under 154 MPa using a KBr pellet kit and hydraulic press (Specac).

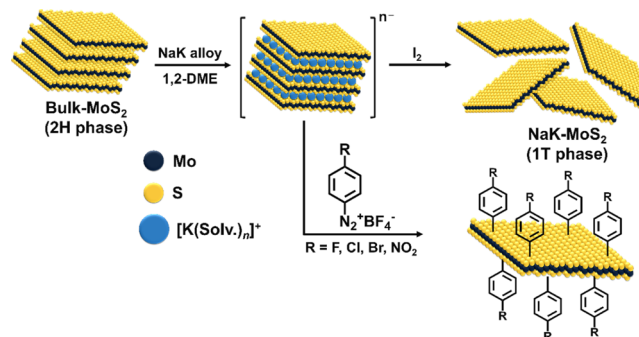
Elemental analysis was performed using a TRUSPEC CHNS microanalyzer, which is able to determinate the contents of C, H, N, and S by combustion of the sample at 1100 °C under an oxygen atmosphere and with the quantitative detection of the combustion products. Before the sample analysis, the determination of blanks was performed (in absence of samples) to check the detection levels of the device. The maximum values of the verified blanks are the following: 0.06% for C, 0.16% of H, 0.02% for N, and 0.35% for S.

SERS Measurements. The SERS substrates were prepared on 300 nm SiO₂/Si surfaces after the cleaning procedure with ethanol and Milli-Q water. NaK-MoS₂ and Li-MoS₂ were dispersed in Milli-Q water for 1 h, and then, MoS₂ dispersions (1 mg mL⁻¹) were covered by drop casting onto the cleaned SiO₂/Si (~25 mm²) surfaces. The substrates were dried at room temperature and then incubated in the different concentrations of R6G and CV solutions for 2 h. The R6G and CV-deposited MoS₂ substrates were washed with Milli-Q water to remove the free R6G or CV and dried under nitrogen atmosphere. Bulk-MoS₂ was also exfoliated by sonication for 1 h to obtain few-layered material for comparison of the SERS activity with NaK-MoS₂ and Li-MoS₂. Afterward, the bulk-MoS₂ substrate was also prepared according to the same preparation procedure mentioned above for SERS measurements. The SERS spectra of so-prepared bulk-MoS₂, NaK-MoS₂, and Li-MoS₂ substrates were recorded using a 100× objective (NA = 0.85) at excitation wavelengths of 532 nm (0.9 mW power laser, 30 s of integration time), 633 nm (0.9 mW power laser, 30 s of integration time), and 785 nm (1.7 mW power laser, 10 s of integration time in scanning mode). The presented spectra were baseline corrected and normalized to the same laser power and integration time. The enhancement factor (EF) value of the fabricated MoS₂ substrates was estimated according to the eq S1.²⁹

RESULTS AND DISCUSSIONS

Phase Engineering by Chemical Exfoliation. Exfoliated and functionalized MoS₂ sheets were synthesized using NaK alloy intercalation (Scheme 1), as detailed in the Experimental

Scheme 1. Schematic Representation of Chemical Exfoliation and Functionalization for MoS₂ with High 1T Phase Ratio



section. Briefly, the exfoliation mechanism of bulk-MoS₂, which is a 2H polytype, can be explained by the intercalation of cations between layers of MoS₂.²⁷ First, bulk-MoS₂ is reduced with solvated electrons, which are generated from the very potent electron source NaK alloy dissolved in DME at room temperature. The initially formed solvated electrons would be consumed by the bulk-MoS₂ and further reduction proceeds until the maximum ratio of cations to MoS₂ is reached. Thus, the exfoliation process is produced by Coulombic repulsion between layers of reduced MoS₂. The negative charges on MoS₂ are balanced by solvated and intercalated Na⁺ or/and K⁺ cations. In addition, the phase of TMDs depends strongly on the d orbital electron density of the transition metal.⁸ As a consequence of the reduction process of bulk-MoS₂, the electron density in the d orbital is increased, leading to a strong structural reorientation, from the thermodynamically more stable semiconducting 2H polytype to the metallic 1T polytype. Finally, the negatively charged MoS₂ is quenched by I₂ as electrophile to obtain an exfoliated material NaK-MoS₂ with a high proportion of 1T phase. For comparison purposes, MoS₂ was also exfoliated by *n*-BuLi (Li-MoS₂) as a conventional intercalating agent for MoS₂ exfoliation.²¹

Chemically exfoliated MoS₂ was studied by XRD, Raman spectroscopy, XPS, UV, TGA, and TEM. The chemical exfoliation of MoS₂ was confirmed by XRD. Figure S2 indicates typical 2θ values of bulk MoS₂ and NaK-MoS₂, with the characteristic sharp (002) diffraction peak of bulk-MoS₂ at 14.5°, shifted to 14.2° and broadened (Figure 1A), indicating the expansion of the interlayer distance and successful exfoliation of MoS₂.^{11,30} In addition, TEM images of NaK-MoS₂ demonstrated few layers of MoS₂ with relatively small lateral dimensions, in the nanometer size range (Figure S24B). HRTEM images showed well-ordered and well-oriented crystalline structuring in the sample, which allows the acquisition of SAED patterns from individual sheets (Figure S25). The crystal structure of NaK-MoS₂ was determined by selected area electron diffraction (Figure S25B), confirming the lattice spacing for our structure to coincide accurately with published reference data for MoS₂.^{31–33}

Raman spectroscopy was used to characterize the change in crystallinity. Figure 1B shows the Raman spectra of bulk-MoS₂ and NaK-MoS₂ excited at 633 nm. In the spectrum of bulk-MoS₂, we observed the two main phonon peaks located at ~380 and ~405 cm⁻¹, arising from the E_{2g} (in-plane) and A_{1g} (out-of-plane) vibration modes of MoS₂, respectively. In addition, a typical second-order longitudinal acoustic phonon

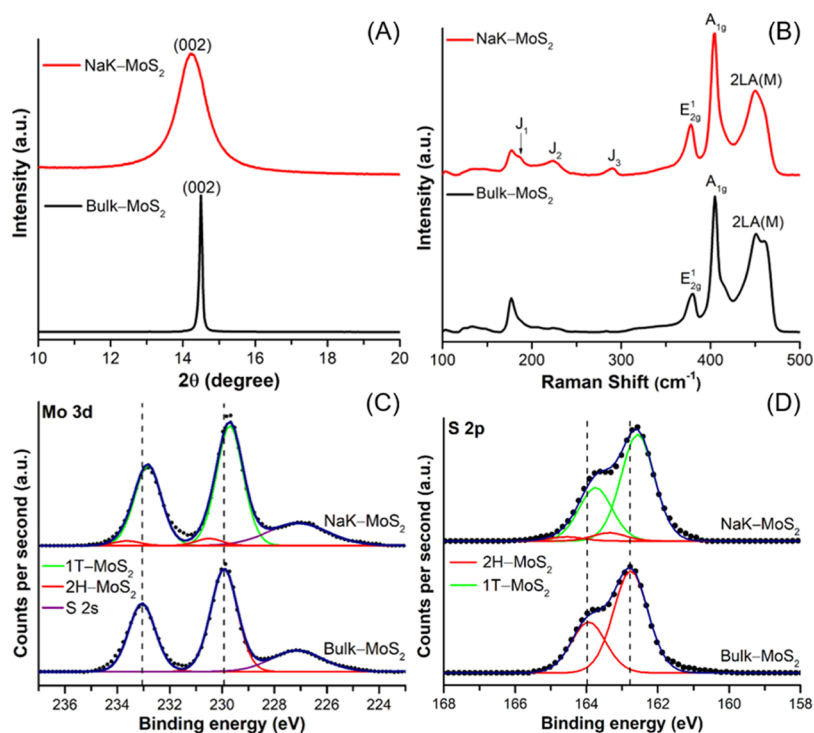


Figure 1. (A) Magnified XRD patterns of the (002) peaks of bulk-MoS₂ and NaK-MoS₂ crystals; (B) Raman spectra of bulk-MoS₂ and NaK-MoS₂ obtained by excitation at 633 nm; (C,D) XPS core level spectra of Mo 3d (~25 meV shift) and S 2p (~24 meV shift) for bulk-MoS₂ and NaK-MoS₂.

peak (2LA(M)) around ~450 cm⁻¹ was also detected. After chemical exfoliation, new peaks were observed at 187, 224, 289 cm⁻¹, which correspond to the J₁–J₃ phonon modes of NaK-MoS₂, respectively. These low-frequency phonon modes confirm that NaK-MoS₂ has 1T phase features, and is in line with the characterization of Li-MoS₂ (Figure S3) and with previously reported values.^{24,34}

In the UV spectrum of bulk-MoS₂ (Figure S4), the two excitonic A and B bands, which are related to the presence of a highly ordered structure, were observed.^{35,36} These characteristic bands disappeared after exfoliation of MoS₂ by NaK alloy, confirming a change in the crystallinity from 2H to 1T MoS₂.¹⁷

The XPS analysis was employed to obtain the MoS₂ 1T/2H ratio, by fitting Mo 3d and S 2p core levels. Sharp Mo 3d signals at 233.05 (Mo 3d^{3/2}) and 229.92 (Mo 3d^{5/2}) were observed in bulk-MoS₂; however, the corresponding signals after exfoliation were shifted (~25 meV) to lower binding energies, suggesting the existence of both 1T and 2H phases after exfoliation (Figure 1C,D). The 1T phase was identified by a shift (~0.8 eV) with respect to that for 2H phase in the fitting of Mo 3d for NaK-MoS₂. A similar XPS result was obtained for Li-MoS₂ (Figure S5); but deconvolution of the Mo 3d peak shows two new peaks for MoO₃ and MoO₂ in Li-MoS₂, whereas NaK-MoS₂ does not display any significant peak from oxidized products of MoS₂. We hypothesize that this may be due to the quenching agent (H₂O) used in the preparation of Li-MoS₂.^{24,34,37}

Upon deconvolution of the corresponding Mo 3d core level, the 1T phase ratio was found to be ~94.5% for NaK-MoS₂ (Table 1). Such a high value indicates that NaK alloy is a suitable intercalating agent, more efficient than Li, and single Na or K.^{19,22} Several factors are crucial for successful exfoliation and phase conversion of TMDs. For instance, Loh et al. reported the high influence of the cation species of

Table 1. Ratio of 1T Phase for Exfoliated and Functionalized Samples, Based on Integrated Areas of Mo 3d Core Level Spectra^b

sample	2H (%)	1T (%)
bulk-MoS ₂	100	
NaK-MoS ₂	5.5	94.5
Li-MoS ₂ ^a	19.0	59.0
MoS ₂ /p-(F)Ph	11.2	88.8
MoS ₂ /p-(Cl)Ph	13.9	86.1
MoS ₂ /p-(Br)Ph	11.1	88.9
MoS ₂ /p-(NO ₂)Ph	20.7	79.3

^aBibliographic data from ref 21. ^bLi-MoS₂ additionally presents 22% of MoO₃ and MoO₂.

alkali metal naphthalenides in the exfoliation efficiency of TMDs, Na⁺ being more efficient than Li⁺ and K⁺.¹⁹ More recently, Sofer et al. also reported that the cation size of intercalating agents is a dominating factor for phase engineering, with smaller cation species showing a better exfoliation and 1T phase conversion for electrochemically exfoliated TMDs.²² However, other parameters such as dispersibility of intercalating agents must be considered for an efficient chemical exfoliation and phase conversion. Comparing NaK alloy with single Na or K, the alkali alloy (which is a liquid) is more easily dispersed in solution than Na or K solid metals at room temperature under stirring conditions, thus leading to higher intercalation and conversion efficiencies than individual Na or K.

SERS Performance. To show the effect of the phase transition from 2H to 1T on the SERS efficiency, a NaK-MoS₂ substrate was prepared on a 300 nm SiO₂/Si surface and compared to MoS₂ exfoliated by *n*-BuLi (Li-MoS₂)²¹ and to bulk-MoS₂, in the detection of rhodamine 6G (R6G) and CV

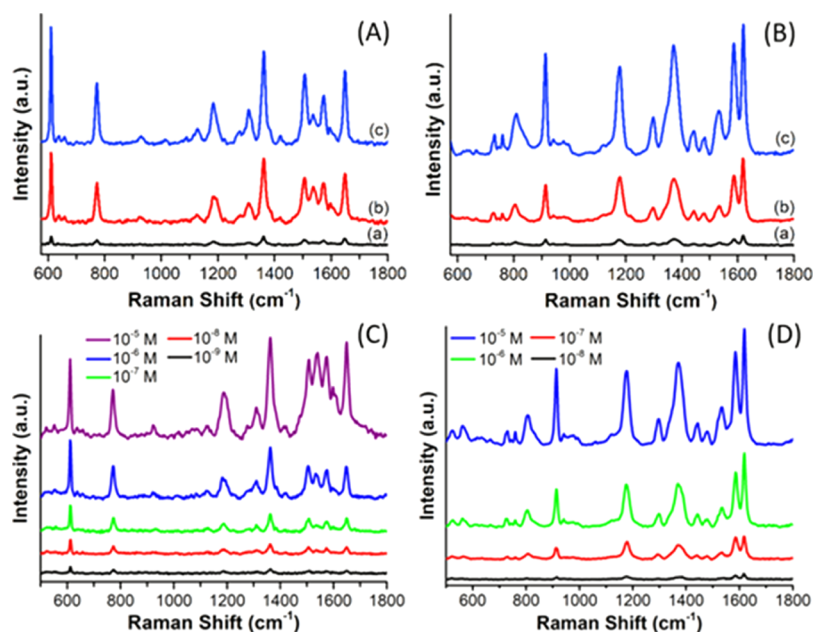


Figure 2. SERS spectra of 10 μ M R6G (A) and CV (B) on bulk-MoS₂ (a), Li-MoS₂ (b), and NaK-MoS₂ (c) substrates, excited by 532 nm laser; SERS spectra of various concentrations of R6G (C) and CV (D), deposited on NaK-MoS₂.

as target analytes. Figure 2A,B displays the SERS spectra of CV and R6G on three MoS₂ modifications excited at 532 nm. The main vibrations of CV were recorded at 1618, 1583, 1378, 1175 (symmetric and asymmetric in-plane CC ring stretch modes), and 914 cm⁻¹ (out-of-plane CC ring bending mode). The most intense R6G vibrations were found at 1647, 1575, 1363 (in-plane CC ring stretch modes), 775, and 611 cm⁻¹ (out-of-plane CC ring bending modes). The results indicate that exfoliated MoS₂ samples provided a significantly higher SERS enhancement than bulk-MoS₂ for both probe molecules (Table 2). The EF of the prepared substrates was calculated to

Table 2. Calculated EFs for bulk-MoS₂, Li-MoS₂, and NaK-MoS₂ Substrates on Different Raman Dyes

dyes	Raman shift (cm ⁻¹)	EFs		
		bulk-MoS ₂	Li-MoS ₂	NaK-MoS ₂
R6G	611	2.04 × 10 ³	1.73 × 10 ⁴	2.92 × 10 ⁴
CV	1618	2.12 × 10 ³	1.39 × 10 ⁴	2.87 × 10 ⁴

evaluate their SERS efficiency using 10 μ M Raman dye solutions, according to the eq S1 (details are given in Supporting Information). NaK-MoS₂ showed an EF 1 order of magnitude higher than bulk-MoS₂ and 2 times higher than Li-MoS₂, for both R6G and CV. Interestingly, the difference between the EFs of NaK-MoS₂ and Li-MoS₂ practically coincides with the difference between their 1T ratios, indicating a higher conductivity which corresponds to a higher-lying Fermi level and provides more efficient CT from the substrate to probe molecules.^{38,39}

The SERS performance of the NaK-MoS₂ substrate was also estimated by evaluating the detection limits for R6G and CV. As shown in Figure 2C,D, the SERS intensity is directly correlated to the concentrations of Raman probes. Although Yin et al. and Anbazhangan et al. reported the use of MoS₂ with a high 1T phase ratio, as SERS substrates for R6G and CV detection,^{10,17} we demonstrate here superior SERS sensitivities for both R6G and CV, using NaK-MoS₂. The lowest detected

concentrations for R6G and CV on NaK-MoS₂ were as low as 10⁻⁹ and 10⁻⁸ M, respectively, which compare favorably with previously reported studies,^{10,17,40,41} and are even comparable to efficient metallic substrates.^{42,43}

Trying to understand in more the depth the origin of such an unusually strong SERS effect for NaK-MoS₂, UV, photoluminescence (PL), and Raman scattering were measured. As mentioned above, contributions to SERS may be of both EM nature, due to excitation of localized surface plasmons, and of chemical nature (CE), due to the probe-substrate interactions providing CT and molecular resonances. The EM mechanism can be nearly excluded because of the absence of strong plasmons or excitons in the UV–vis spectrum (Figures 3 and S4). The quenching of the intrinsic absorbance and PL of CV and R6G with increasing NaK-MoS₂ concentration indicates a strong coupling between probe and substrate, leading to effective (nonradiative) CT resonances (Figures S10–S13). Measurements of R6G and CV using 532, 633, and 785 nm excitation wavelengths revealed that only strong SERS signals were recorded when the laser was in resonance with an electronically excited state of the probe, or close to it. In addition, we note that no Raman signals were detected when using other probe molecules such as mercaptobenzoic acid (data not shown), which can be readily measured on metal nanostructures.^{44–46} In conclusion, all these experimental data suggest as the major cause of SERS is the CE mechanism. The molecular resonances were identified by UV–vis spectroscopy to be around 527 nm in R6G (Figure 3A) and around 595 nm, with a prominent shoulder around 545 nm, in CV (Figure 3B). The difference between the UV–vis spectra of NaK-MoS₂ in the presence and absence of the dyes did not display new resonances close to the excitation wavelengths, but in the case of CV, the 7 nm (blue) shift of the 545 nm shoulder indicated significant binding of the molecule to the surface, concomitantly pushing the resonance maximum close toward the 532 nm excitation wavelength. This, in turn, could explain the relatively high SERS intensity of CV at 532 nm.

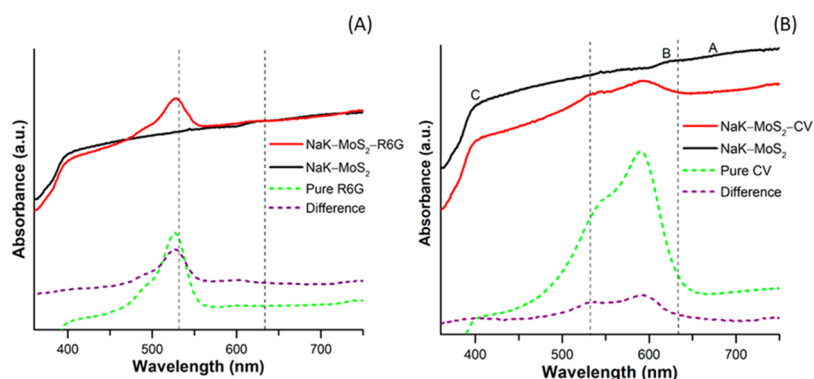


Figure 3. UV-vis absorbance spectra of dye-NaK-MoS₂ (red line) and pure NaK-MoS₂ (black line) suspensions compared to pure dye solutions (green line) containing 1 μ M R6G and 20 mg mL⁻¹ NaK-MoS₂ (A) and 1 μ M CV and 20 mg mL⁻¹ NaK-MoS₂ (B). Dashed, vertical lines (gray) highlight available laser excitation wavelengths. The difference spectrum between the dye-NaK-MoS₂ and NaK-MoS₂ (purple lines) reveal that the excitation of the molecular resonances of adsorbed dyes is partially quenched by the presence of NaK-MoS₂, indicating effective interaction with the MoS₂ substrate.

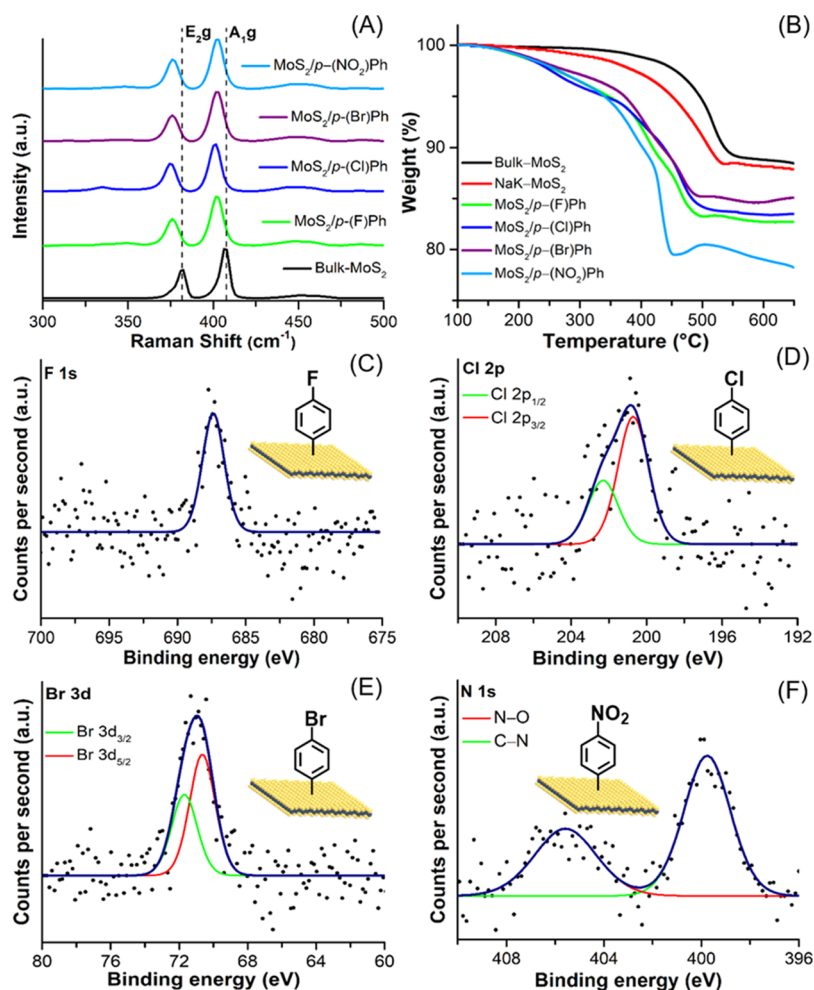


Figure 4. (A) Raman spectra of bulk-MoS₂, MoS₂/p-(F)Ph, MoS₂/p-(Cl)Ph, MoS₂/p-(Br)Ph, and MoS₂/p-(NO₂)Ph at 633 nm; (B) TGA profiles of bulk-MoS₂, NaK-MoS₂, MoS₂/p-(F)Ph, MoS₂/p-(Cl)Ph, MoS₂/p-(Br)Ph and MoS₂/p-(NO₂)Ph from 100 to 650 °C under air; core level spectra of (C) F 1s, (D) Cl 2p, (E) Br 3d and (F) N 1s for MoS₂/p-(F)Ph, MoS₂/p-(Cl)Ph, MoS₂/p-(Br)Ph and MoS₂/p-(NO₂)Ph.

The SERS mechanism can thus be explained by the excitation of a molecular resonance coupled with electron transfer from the Fermi level of the substrate into the molecule. As the Fermi level E_F of NaK-MoS₂ ($E_F = -5.0$ eV) lies energetically above the HOMO of both dyes (E_{HOMO} , CV = -6.0 eV and E_{HOMO} , R6G = -5.7 eV),¹⁷ the subsequent CT

from E_F to the HOMO does not require extra energy and thus is strongly favored. This eventually results in a greatly enhanced electron transition probability, leading to high signal intensities for R6G and CV at 532 nm. At 633 nm excitation, a preresonance condition originates strong CV intensities, whereas no R6G signal can be measured because it is off-

resonance with the molecular excitation. The absence of electronically excited states in both dye molecules at 785 nm and the consequently missing SERS signals are in line with this interpretation (Figure S6). Further, the extraordinarily large enhancement of the vibrational out-of-plane modes at 611 and 775 cm^{-1} in R6G and the mode at 914 cm^{-1} in CV, compared to the in-plane modes, are related to vibronic coupling between a molecular resonance and CT state.^{47,48}

The reproducibility and signal homogeneity are also important parameters for SERS substrates in routine analytical applications. The homogeneity of the SERS signals for R6G at 611 cm^{-1} and CV at 1620 cm^{-1} on NaK-MoS₂ was studied by Raman mapping (Figures S7–S9). To evaluate the reproducibility for R6G and CV, we randomly collected SERS spectra from 20 different positions on the same NaK-MoS₂ substrate (Figures S8 and S9). The results indicate uniform and reproducible SERS signals over the whole surface, which is likely related to homogenous and efficient capture of the probe molecules.

Chemical Modification. In addition, chemical exfoliation by intercalation of metal ions is highly versatile because it allows carrying out chemical modifications on the exfoliated MoS₂ structure.⁷ The chemical modification of 2D-based materials is of high interest, as it allows modifying chemical and physical properties such as conductivity, stability, and reactivity.^{49,50}

In general, the functionalization of MoS₂ is typically achieved by exploiting sulfur vacancies or defects occurring on the surface during chemical exfoliation. Recently, Pérez et al. reported a versatile mild covalent functionalization at basal planes of exfoliated 2H-MoS₂ and WS₂ through the nucleophilic attack of sulfur atoms from the metal transition dichalcogenide structure on maleimide derivatives.⁵¹ M. Pumera et al. reported a highly efficient modification of MoS₂ in water with thiobarbituric acid by nucleophilic attack of its sulfur on the exfoliated MoS₂ material.⁵² 1T-MoS₂ presents a higher chemical reactivity toward functionalization, especially at basal sites, as compared to 2H-MoS₂.⁵³ Voiry et al. successfully functionalized the surface of 1T-MoS₂ via the covalent attachment of organohalide functional groups.²⁵ Chemically exfoliated MoS₂ can also be covalently functionalized by aryl diazonium compounds. Knirsch et al. and Benson et al. reported a well-known chemical approach, which does not rely on structural defects, to functionalize the surface of chemically exfoliated 1T-MoS₂ with substituted phenyl diazonium salts.^{24,34} Thus, the negatively charged 1T phase MoS₂ nanolayers obtained by treatment with NaK alloy were functionalized with different para (*p*)-substituted aryl diazonium salts, thereby demonstrating the versatility of the proposed reaction on the MoS₂ surface. For this purpose, we selected four para-substituted (R: F, Cl, Br, and NO₂) aryl diazonium salts with heteroatoms because they can be readily analyzed by XPS. We refer to MoS₂ functionalized with para F, Cl, Br, or NO₂-phenyl rings as MoS₂/*p*-(F)Ph, MoS₂/*p*-(Cl)Ph, MoS₂/*p*-(Br)Ph, or MoS₂/*p*-(NO₂)Ph, respectively. It is worth mentioning that, in principle, substituents of phenyl groups would not be reduced by the NaK alloy during the reaction because the same amount of diazonium compounds and NaK alloy were used, and the diazonium group is more readily reduced.^{34,53}

Chemically functionalized MoS₂ derivatives were characterized by Raman spectroscopy, XPS, FTIR, TGA, and TEM. In Raman spectroscopy, all functionalized MoS₂ samples were

found to display the expected transitions around at 376 cm^{-1} (E_{2g}) and 402 cm^{-1} (A_{1g}) and also to have weak Raman peaks for J₁, J₂, and J₃ modes, indicating the presence of the 1T phase after functionalization (Figure 4A).³⁴ The covalent functionalization of MoS₂ layers was also confirmed by FTIR (Figure S14). All functionalized samples showed the characteristic C=C stretching bands of benzene rings located around 1640 cm^{-1} and the weak C–S stretching bands between 620 and 690 cm^{-1} , suggesting that the benzene moieties were covalently attached to the MoS₂ surface via C–S bonds. Additionally, MoS₂/*p*-(NO₂)Ph presented two main bands at 1504 and 1330 cm^{-1} , which were attributed to characteristic asymmetric and symmetric stretching of a nitro group attached to the phenyl moiety.

The thermal properties and FD of chemically exfoliated and derivative MoS₂ samples were investigated by TGA in air. Figure 4B shows that 2H-MoS₂ started to lose weight at approximately 350 °C, which is attributed to partial oxidation of MoS₂ into MoO₃. In addition, the surface functional groups were decomposed in the range of 200–500 °C, as expected (Table 3). The second rapid weight loss (>50% wt) in all

Table 3. FD of 1T-MoS₂ Nanosheets Obtained by TGA

functional group	weight loss (%) ^a	FD ^b
<i>p</i> -NO ₂ -C ₆ H ₄	11.5	5.9
<i>p</i> -F-C ₆ H ₄	6.5	8.6
<i>p</i> -Cl-C ₆ H ₄	5.6	9.1
<i>p</i> -Br-C ₆ H ₄	7.2	16.5

^aDetermined weight loss at 650 °C. ^bNumber of MoS₂ molecules per functional group

samples was attributed to the decomposition of MoS₂ by sublimation of MoO₃ (Figure S16).^{54,55} The FD for all functionalized samples was calculated by considering the decomposition of MoS₂ at 650 °C, according to eq 1.

The results suggest that the reactivity of the diazonium compounds is related to the substituted groups in the phenyl ring (Br < Cl < F < NO₂). This trend can be explained by the single-electron transfer reaction mechanism from negatively charged MoS₂ to the diazonium compound, being reduced to the corresponding aryl radical.⁴⁴ The lower reduction potentials of the employed diazonium salts are caused by the stronger electron-withdrawing substituted groups in the phenyl ring (Br < Cl < F < NO₂), improving the electron transfer process, which is in agreement with previous results for carbon nanotubes.⁵⁶

The XPS analysis was used to study the atomic composition of MoS₂ surfaces (Figures S17–S22). XPS was first employed to provide evidence for the functionalization of MoS₂ derivatives, by identifying and quantifying the functional groups anchored to the surface (Table S2). Bulk-MoS₂ is not expected to contain C and O in the bulk material; however, the undesired C and O content probably arises from CO and CO₂ species in air, adsorbed on the substrates. Such C and O contents were detected by XPS in the starting material and in the rest of functionalized MoS₂ samples, with the same proportion. The presence of F, Cl, Br, and N was detected after chemical modification in the atomic composition of MoS₂/*p*-(F)Ph (1.0%), MoS₂/*p*-(Cl)Ph (0.9%), MoS₂/*p*-(Br)Ph (0.7%), and MoS₂/*p*-(NO₂)Ph (3.8%), respectively. Besides, the deconvolution of F 1s, Cl 2p, Br 3d, and N 1s for MoS₂/*p*-(F)Ph, MoS₂/*p*-(Cl)Ph, MoS₂/*p*-(Br)Ph, and MoS₂/*p*-(NO₂)-

Ph, respectively, showed spectral components from C–F (687.4 eV), C–Cl (200.9 eV), C–Br (71.0 eV), and C–NO₂ (399.8 and 405.6 eV, Figure 4C–F). The presence of these chemical bonds on the corresponding MoS₂ surfaces confirmed functionalization. The obtained XPS results are in agreement with related functionalization approaches in the literature,^{24,25,34,53} confirming the presence of p-substituted benzene functional groups on MoS₂ layers. TEM images indicate that functionalized MoS₂ derivatives keep dimensions similar to those of exfoliated material after chemical modification (Figures S24C–F). The elemental analysis of the different modified MoS₂ derivatives was performed to calculate the FD with respect to the C/S atom ratio (Table S3). The C/S ratios of functionalized materials were higher than those for NaK-MoS₂ because of the introduction of phenyl groups on the MoS₂ surfaces.

CONCLUSIONS

In conclusion, we report a novel approach for exfoliation and covalent functionalization of MoS₂, which provides a remarkably efficient phase modification, by using NaK alloys. The proposed exfoliation method leads to highly enriched 1T phase MoS₂ (94.5%). MoS₂ was chemically functionalized by radical reactions with different phenyl diazonium compounds, leading to MoS₂ enriched in metallic 1T phase. NaK-MoS₂ revealed a remarkable SERS enhancement on R6G and CV, because of an efficient CE mechanism, which may open the way toward further sensing applications. Work is in progress to explore the limits of this approach, in terms of reactivity, physical properties of the obtained enriched 1T phase MoS₂ materials (e.g., electrical conductivity, optical properties, etc.), and sensing applications.

ASSOCIATED CONTENT

Supporting Information

The Supporting Information is available free of charge on the ACS Publications website at DOI: 10.1021/acs.chemmater.9b01698.

Experimental details on the preparation and characterization of the different para-substituted benzenediazonium tetrafluoroborates; XRD data; Raman spectra, UV–vis adsorption spectra, XPS analysis of bulk-MoS₂, Li-MoS₂, and NaK-MoS₂; estimation of the EF, SERS spectra, SERS reproducibility, UV–vis adsorption spectra, and PL spectra of NaK-MoS₂ with R6G and CV; and FTIR data, TGA data, Raman spectra, XPS analysis, combustion elemental analysis, and TEM images of the different MoS₂ derivatives (PDF)

AUTHOR INFORMATION

Corresponding Authors

*E-mail: acriado@cicbiomagune.es (A.C.).

*E-mail: prato@units.it (M.P.).

ORCID

Hui-Lei Hou: 0000-0002-8004-0541

Alejandro Criado: 0000-0002-9732-513X

Marco Möller: 0000-0001-7554-4799

Luis M. Liz-Marzán: 0000-0002-6647-1353

Maurizio Prato: 0000-0002-8869-8612

Notes

The authors declare no competing financial interest.

ACKNOWLEDGMENTS

M.P. is the recipient of the AXA Chair (2016–2023). A.C. thanks MINECO for his researcher grant (Juan de la Cierva—Incorporación). E.E. is grateful for a fellowship from the Scientific and Technological Research Council of Turkey (TUBITAK). This work was supported by the Graphene Flagship Core 2 grant agreement no. 785219. This work was performed under the Maria de Maeztu Units of Excellence Program from the Spanish State Research Agency—grant no. MDM-2017-0720.

REFERENCES

- (1) Li, Y.; Wang, H.; Xie, L.; Liang, Y.; Hong, G.; Dai, H. MoS₂ Nanoparticles Grown on Graphene: An Advanced Catalyst for the Hydrogen Evolution Reaction. *J. Am. Chem. Soc.* **2011**, *133*, 7296–7299.
- (2) Lee, K.; Gatensby, R.; McEvoy, N.; Hallam, T.; Duesberg, G. S. High-Performance Sensors Based on Molybdenum Disulfide Thin Films. *Adv. Mater.* **2013**, *25*, 6699–6702.
- (3) Chhowalla, M.; Shin, H. S.; Eda, G.; Li, L.-J.; Loh, K. P.; Zhang, H. The Chemistry of Two-Dimensional Layered Transition Metal Dichalcogenide Nanosheets. *Nat. Chem.* **2013**, *5*, 263–275.
- (4) Radisavljevic, B.; Radenovic, A.; Brivio, J.; Giacometti, V.; Kis, A. Single-layer MoS₂ transistors. *Nat. Nanotechnol.* **2011**, *6*, 147–150.
- (5) Jia, Q.; Huang, X.; Wang, G.; Diao, J.; Jiang, P. MoS₂ Nanosheet Superstructures Based Polymer Composites for High-Dielectric and Electrical Energy Storage Applications. *J. Phys. Chem. C* **2016**, *120*, 10206–10214.
- (6) Conley, H. J.; Wang, B.; Ziegler, J. I.; Haglund, R. F.; Pantelides, S. T.; Bolotin, K. I. Bandgap Engineering of Strained Monolayer and Bilayer MoS₂. *Nano Lett.* **2013**, *13*, 3626–3630.
- (7) Yu, Y.; Nam, G.-H.; He, Q.; Wu, X.-J.; Zhang, K.; Yang, Z.; Chen, J.; Ma, Q.; Zhao, M.; Liu, Z.; et al. High phase-purity 1T'-MoS₂- and 1T'-MoSe₂-layered crystals. *Nat. Chem.* **2018**, *10*, 638–643.
- (8) Voiry, D.; Mohite, A.; Chhowalla, M. Phase Engineering of Transition Metal Dichalcogenides. *Chem. Soc. Rev.* **2015**, *44*, 2702–2712.
- (9) Lukowski, M. A.; Daniel, A. S.; Meng, F.; Forticaux, A.; Li, L.; Jin, S. Enhanced Hydrogen Evolution Catalysis from Chemically Exfoliated Metallic MoS₂ Nanosheets. *J. Am. Chem. Soc.* **2013**, *135*, 10274–10277.
- (10) Anbazhagan, R.; Vadivelmurugan, A.; Tsai, H.-C.; Jeng, R.-J. Surface-Enhanced Raman Scattering of Alkyne-Conjugated MoS₂: A Comparative Study between Metallic and Semiconductor Phases. *J. Mater. Chem. C* **2018**, *6*, 1071–1082.
- (11) Acerce, M.; Voiry, D.; Chhowalla, M. Metallic 1T phase MoS₂ nanosheets as supercapacitor electrode materials. *Nat. Nanotechnol.* **2015**, *10*, 313–318.
- (12) Luxa, J.; Vosecký, P.; Mazánek, V.; Sedmidubský, D.; Pumera, M.; Lazar, P.; Sofer, Z. Layered Transition-Metal Ditellurides in Electrocatalytic Applications—Contrasting Properties. *ACS Catal.* **2017**, *7*, 5706–5716.
- (13) Cialla-May, D.; Zheng, X.-S.; Weber, K.; Popp, J. Recent Progress in Surface-Enhanced Raman Spectroscopy for Biological and Biomedical Applications: From Cells to Clinics. *Chem. Soc. Rev.* **2017**, *46*, 3945–3961.
- (14) Baik, S. Y.; Cho, Y. J.; Lim, Y. R.; Im, H. S.; Jang, D. M.; Myung, Y.; Park, J.; Kang, H. S. Charge-Selective Surface-Enhanced Raman Scattering Using Silver and Gold Nanoparticles Deposited on Silicon-Carbon Core-Shell Nanowires. *ACS Nano* **2012**, *6*, 2459–2470.
- (15) Otto, A. The 'chemical' (electronic) contribution to surface-enhanced Raman scattering. *J. Raman Spectrosc.* **2005**, *36*, 497–509.
- (16) Muehlethaler, C.; Considine, C. R.; Menon, V.; Lin, W.-C.; Lee, Y.-H.; Lombardi, J. R. Ultrahigh Raman Enhancement on Monolayer MoS₂. *ACS Photonics* **2016**, *3*, 1164–1169.

- (17) Yin, Y.; Miao, P.; Zhang, Y.; Han, J.; Zhang, X.; Gong, Y.; Gu, L.; Xu, C.; Yao, T.; Xu, P.; et al. Significantly Increased Raman Enhancement on MoX₂ (X = S, Se) Monolayers upon Phase Transition. *Adv. Funct. Mater.* **2017**, *27*, 1606694.
- (18) Jung, Y.; Zhou, Y.; Cha, J. J. Intercalation in Two-Dimensional Transition Metal Chalcogenides. *Inorg. Chem. Front.* **2016**, *3*, 452–463.
- (19) Zheng, J.; Zhang, H.; Dong, S.; Liu, Y.; Tai Nai, C.; Suk Shin, H.; Young Jeong, H.; Liu, B.; Ping Loh, K. High Yield Exfoliation of Two-Dimensional Chalcogenides Using Sodium Naphthalenide. *Nat. Commun.* **2014**, *5*, 2995.
- (20) Ding, W.; Hu, L.; Dai, J.; Tang, X.; Wei, R.; Sheng, Z.; Liang, C.; Shao, D.; Song, W.; Liu, Q.; et al. Highly Ambient-Stable 1T-MoS₂ and 1T-WS₂ by Hydrothermal Synthesis under High Magnetic Fields. *ACS Nano* **2019**, *13*, 1694.
- (21) Chen, Z.; Leng, K.; Zhao, X.; Malkhandi, S.; Tang, W.; Tian, B.; Dong, L.; Zheng, L.; Lin, M.; Yeo, B. S.; et al. Interface Confined Hydrogen Evolution Reaction in Zero Valent Metal Nanoparticles-Intercalated Molybdenum Disulfide. *Nat. Commun.* **2017**, *8*, 14548.
- (22) Luxa, J.; Vosecký, P.; Mazánek, V.; Sedmidubský, D.; Pumera, M.; Sofer, Z. Cation-Controlled Electrocatalytic Activity of Transition-Metal Disulfides. *ACS Catal.* **2018**, *8*, 2774–2781.
- (23) Englert, J. M.; Dotzer, C.; Yang, G.; Schmid, M.; Papp, C.; Gottfried, J. M.; Steinrück, H.-P.; Spiecker, E.; Hauke, F.; Hirsch, A. Covalent Bulk Functionalization of Graphene. *Nat. Chem.* **2011**, *3*, 279–286.
- (24) Knirsch, K. C.; Berner, N. C.; Nerl, H. C.; Cucinotta, C. S.; Gholamvand, Z.; McEvoy, N.; Wang, Z.; Abramovic, I.; Vecera, P.; Halik, M.; et al. Basal-Plane Functionalization of Chemically Exfoliated Molybdenum Disulfide by Diazonium Salts. *ACS Nano* **2015**, *9*, 6018–6030.
- (25) Voiry, D.; Goswami, A.; Kappera, R.; Silva, C. D. C. C. E.; Kaplan, D.; Fujita, T.; Chen, M.; Asefa, T.; Chhowalla, M. Covalent Functionalization of Monolayered Transition Metal Dichalcogenides by Phase Engineering. *Nat. Chem.* **2015**, *7*, 45–49.
- (26) El Garah, M.; Bertolazzi, S.; Ippolito, S.; Eredia, M.; Janica, I.; Melinte, G.; Ersen, O.; Marletta, G.; Ciesielski, A.; Samori, P. MoS₂ nanosheets via electrochemical lithium-ion intercalation under ambient conditions. *FlatChem* **2018**, *9*, 33–39.
- (27) Feng, H.; Hu, Z.; Liu, X. Facile and Efficient Exfoliation of Inorganic Layered Materials Using Liquid Alkali Metal Alloys. *Chem. Commun.* **2015**, *51*, 10961–10964.
- (28) Hou, H.-L.; Dasler, D.; Hauke, F.; Hirsch, A. Reductive Functionalization of Graphenes With Nickel(II) Porphyrin Diazonium Compounds. *Phys Status Solidi—Rapid Res. Lett.* **2017**, *11*, 1700306.
- (29) Tao, W.; Zhao, A.; Sun, H.; Gan, Z.; Zhang, M.; Li, D.; Guo, H. Periodic Silver Nanodishes as Sensitive and Reproducible Surface-Enhanced Raman Scattering Substrates. *RSC Adv.* **2014**, *4*, 3487–3493.
- (30) Jiang, L.; Zhang, S.; Kulinich, S. A.; Song, X.; Zhu, J.; Wang, X.; Zeng, H. Optimizing Hybridization of 1T and 2H Phases in MoS₂ monolayers to Improve Capacitances of Supercapacitors. *Mater Res Lett* **2015**, *3*, 177–183.
- (31) Fang, Y.; Pan, J.; He, J.; Luo, R.; Wang, D.; Che, X.; Bu, K.; Zhao, W.; Liu, P.; Mu, G.; et al. Structure Re-Determination and Superconductivity Observation of Bulk 1T MoS₂. *Angew. Chem., Int. Ed.* **2018**, *57*, 1232–1235.
- (32) Jana, M. K.; Rao, C. N. R. Two-Dimensional Inorganic Analogues of Graphene: Transition Metal Dichalcogenides. *Philos. Trans. R. Soc. A Math Phys. Eng. Sci.* **2016**, *374*, 20150318.
- (33) Naumov, N. G.; Korlyukov, A. A.; Piryazev, D. A.; Virovets, A. V.; Fedorov, V. E. High-Precision X-Ray Diffraction Data, Experimental and Theoretical Study of 2H-MoS₂. *Russ. Chem. Bull.* **2013**, *62*, 1852–1857.
- (34) Benson, E. E.; Zhang, H.; Schuman, S. A.; Nanayakkara, S. U.; Bronstein, N. D.; Ferrere, S.; Blackburn, J. L.; Miller, E. M. Balancing the Hydrogen Evolution Reaction, Surface Energetics, and Stability of Metallic MoS₂ Nanosheets via Covalent Functionalization. *J. Am. Chem. Soc.* **2018**, *140*, 441–450.
- (35) Pagona, G.; Bittencourt, C.; Arenal, R.; Tagmatarchis, N. Exfoliated semiconducting pure 2H-MoS₂ and 2H-WS₂ assisted by chlorosulfonic acid. *Chem. Commun.* **2015**, *51*, 12950–12953.
- (36) Eda, G.; Yamaguchi, H.; Voiry, D.; Fujita, T.; Chen, M.; Chhowalla, M. Photoluminescence from Chemically Exfoliated MoS₂. *Nano Lett.* **2011**, *11*, 5111–5116.
- (37) Ambrosi, A.; Sofer, Z.; Pumera, M. 2H → 1T phase transition and hydrogen evolution activity of MoS₂, MoSe₂, WS₂ and WSe₂ strongly depends on the MX₂ composition. *Chem. Commun.* **2015**, *51*, 8450–8453.
- (38) Lee, Y.; Kim, H.; Lee, J.; Yu, S. H.; Hwang, E.; Lee, C.; Ahn, J.-H.; Cho, J. H. Enhanced Raman Scattering of Rhodamine 6G Films on Two-Dimensional Transition Metal Dichalcogenides Correlated to Photoinduced Charge Transfer. *Chem. Mater.* **2016**, *28*, 180–187.
- (39) Ling, X.; Fang, W.; Lee, Y.-H.; Araujo, P. T.; Zhang, X.; Rodriguez-Nieva, J. F.; Lin, Y.; Zhang, J.; Kong, J.; Dresselhaus, M. S. Raman Enhancement Effect on Two-Dimensional Layered Materials: Graphene, h-BN and MoS₂. *Nano Lett.* **2014**, *14*, 3033–3040.
- (40) Sun, L.; Hu, H.; Zhan, D.; Yan, J.; Liu, L.; Teguh, J. S.; Yeow, E. K. L.; Lee, P. S.; Shen, Z. Plasma Modified MoS₂ nanoflakes for Surface Enhanced Raman Scattering. *Small* **2014**, *10*, 1090–1095.
- (41) Yan, D.; Qiu, W.; Chen, X.; Liu, L.; Lai, Y.; Meng, Z.; Song, J.; Liu, Y.; Liu, X.-Y.; Zhan, D. Achieving High-Performance Surface-Enhanced Raman Scattering through One-Step Thermal Treatment of Bulk MoS₂. *J. Phys. Chem. C* **2018**, *122*, 14467–14473.
- (42) Zhang, C.; Jiang, S. Z.; Yang, C.; Li, C. H.; Huo, Y. Y.; Liu, X. Y.; Liu, A. H.; Wei, Q.; Gao, S. S.; Gao, X. G.; et al. Gold@silver Bimetal Nanoparticles/Pyramidal Silicon 3D Substrate with High Reproducibility for High-Performance SERS. *Sci. Rep.* **2016**, *6*, 25243.
- (43) Yin, H. J.; Chen, Z. Y.; Zhao, Y. M.; Lv, M. Y.; Shi, C. A.; Wu, Z. L.; Zhang, X.; Liu, L.; Wang, M. L.; Xu, H. J. Ag@Au Core-Shell Dendrites: A Stable, Reusable and Sensitive Surface Enhanced Raman Scattering Substrate. *Sci. Rep.* **2015**, *5*, 14502.
- (44) Li, S.; Zhou, Q.; Chu, W.; Zhao, W.; Zheng, J. Surface-Enhanced Raman Scattering Behaviour of 4-Mercaptophenyl Boronic Acid on Assembled Silver Nanoparticles. *Phys. Chem. Chem. Phys.* **2015**, *17*, 17638–17645.
- (45) Wang, Y.; Polavarapu, L.; Liz-Marzán, L. M. Reduced Graphene Oxide-Supported Gold Nanostars for Improved SERS Sensing and Drug Delivery. *ACS Appl. Mater. Interfaces* **2014**, *6*, 21798–21805.
- (46) Ho, C.-H.; Lee, S. SERS and DFT Investigation of the Adsorption Behavior of 4-Mercaptobenzoic Acid on Silver Colloids. *Colloids Surfaces A Physicochem Eng Asp* **2015**, *474*, 29–35.
- (47) Cañamares, M. V.; Chenal, C.; Birke, R. L.; Lombardi, J. R. DFT, SERS, and Single-Molecule SERS of Crystal Violet. *J. Phys. Chem. C* **2008**, *112*, 20295–20300.
- (48) Hildebrandt, P.; Stockburger, M. Surface-Enhanced Resonance Raman Spectroscopy of Rhodamine 6G Adsorbed on Colloidal Silver. *J. Phys. Chem.* **1984**, *88*, 5935–5944.
- (49) Tang, Q.; Jiang, D.-e. Stabilization and Band-Gap Tuning of the 1T-MoS₂ Monolayer by Covalent Functionalization. *Chem. Mater.* **2015**, *27*, 3743–3748.
- (50) Hirsch, A.; Hauke, F. Post-Graphene 2D Chemistry: The Emerging Field of Molybdenum Disulfide and Black Phosphorus Functionalization. *Angew. Chem., Int. Ed.* **2018**, *57*, 4338–4354.
- (51) Vera-Hidalgo, M.; Giovanelli, E.; Navío, C.; Pérez, E. M. Mild Covalent Functionalization of Transition Metal Dichalcogenides with Maleimides: A “Click” Reaction for 2H-MoS₂ and WS₂. *J. Am. Chem. Soc.* **2019**, *141*, 3767–3771.
- (52) Presolski, S.; Wang, L.; Loo, A. H.; Ambrosi, A.; Lazar, P.; Ranc, V.; Otyepka, M.; Zboril, R.; Tomanec, O.; Ugolotti, J.; Sofer, Z.; Pumera, M. Functional Nanosheet Synthons by Covalent Modification of Transition-Metal Dichalcogenides. *Chem. Mater.* **2017**, *29*, 2066–2073.
- (53) Vishnoi, P.; Sampath, A.; Waghmare, U. V.; Rao, C. N. R. Covalent Functionalization of Nanosheets of MoS₂ and MoSe₂ by

Substituted Benzenes and Other Organic Molecules. *Chem.—Eur. J.* **2017**, *23*, 886–895.

(54) Mahmood, Q.; Park, S. K.; Kwon, K. D.; Chang, S. J.; Hong, J. Y.; Shen, G.; Jung, Y. M.; Park, T. J.; Khang, S. W.; Kim, W. S.; et al. Transition from Diffusion-Controlled Intercalation into Extrinsicly Pseudocapacitive Charge Storage of MoS₂ by Nanoscale Heterostructuring. *Adv. Energy Mater.* **2016**, *6*, 1501115.

(55) Wang, Z.; Chen, T.; Chen, W.; Chang, K.; Ma, L.; Huang, G.; Chen, D.; Lee, J. Y. CTAB-assisted synthesis of single-layer MoS₂-graphene composites as anode materials of Li-ion batteries. *J. Mater. Chem. A* **2013**, *1*, 2202–2210.

(56) Hof, F.; Bosch, S.; Eigler, S.; Hauke, F.; Hirsch, A. New Basic Insight into Reductive Functionalization Sequences of Single Walled Carbon Nanotubes (SWCNTs). *J. Am. Chem. Soc.* **2013**, *135*, 18385–18395.